Journal of Interfaces, Thin films, and Low dimensional systems 2 (2) Winter and Spring (2019) 195-201

Miniband formation engineering in GaN/AlN constant total effective radius multi-shells quantum dots and rings with on-center hydrogenic donor impurities

Mehdi Solaimani and Hadi Johari

Department of Physics, Faculty of Science, Qom University of Technology, Qom, Iran

ARTICLE INFO

Article history:
Received 1 May 2019
Revised 1 May 2020
Accepted 17 May 2020
Available online 20 May 2020

Keywords:
Miniband Engineering
Constant total effective radius multi-shells
Quantum dots and rings
Numerical discretization method

ABSTRACT

In this work, we have studied the miniband and minigaps of GaN/AlN constant total effective radius multi-shells quantum dots (CTER-MSQDs) and Rings (CTER-MSQRs). We have investigated effects of the Hydrogenic donor impurities, quantum dots and rings radii, and the number of wells on miniband formation by sub-band energy calculations. We show that in these systems, minigaps can be created and then disappeared when the number of wells increases. We observe that cylindrical CTER-MSQDs have one miniband more than the spherical CTER-MSQD. However, minibands of the cylindrical CTER-MSQD are wider. For cylindrical systems, the first minigap position can undertake a blue shift but for spherical systems, we can not observe this fact. The first minigap position undertakes more blue shifts when the inner QD radius R1 increases. Thus, the number of wells, Hydrogenic donor impurities, and quantum dot & ring radii can be used as tuning tools to have a system with the typical number of minibands and minigaps with desired widths.

1 Introduction

Confinement of electrons in lower dimension electronic systems can lead to striking modifications of the energy spectrum when compared with the three-dimensional case. The free motion will be quantized into electronic sub-bands [1]. Information about these states can be obtained through different spectroscopies, like tunneling Raman interband optical spectroscopy and intraband infrared spectroscopy.

Well-known periodic structure Superlatices do not exist in the nature. They are formed as a new category of man-made structures proposed by Esaki [2] before being experimentally fabricated [3-4]. Formation of minibands in superlattices led to their outstanding situation in electronic transport investigations during the last few decades [5-6]. In the way of developing the theory of minibands, collapse of the minibands [7-8], and miniband transport phenomena [9-10] for both wide [11] and narrow [12] miniband forms have been investigated. In these studies, the device applications have always been the underlying motivations. Superlattices can have different applications in the fabrication of nano-structured devices such as resonant-tunneling transistors [13], solar cells [14], diodes [15], quantum cascade lasers [16] and detectors [17].

To tune the physical properties of a multi-well system, superlattices with different arranging of building blocks such as Fibonacci [18] and Pascal-type [19]

*Corresponding author.
Email address: Solaimani@Qut.ac.ir
DOI: 10.22051/jitl.2020.25826.1029

superlattices have been studied. Changing of the barrier width in studying of the miniband formation and miniband widths are also the most frequently used methods in the literature [20-21]. Here we have used another approach; our approach is based on retaining the total length of the structure constant and varying the number of wells (Constant Total Effective Length systems). In this way, smaller nano-device sizes (one of the most challenging parameters in modern technologies) and optimized physical properties have become our main motivations. Thus, we have studied the optical properties of constant total effective length multiple quantum well systems [22]. We investigate the physical properties of GaN/AlN constant total effective radius multi-well quantum rings under well number variation effects [23] and the optical properties of two-electron [24] with included impurity [25] GaN/AlN constant total effective radius multi-shell quantum rings and dots, respectively. Along with these investigations, we have studied the miniband formation procedure in GaN/AlN constant total effective radius multi-shell quantum dots [26].

In the present work, we have studied the effect of a hydrogenic donor impurity and number of wells on miniband formation process in GaN/AlN CTER-MSQDs and CTER-MSQRs. Our calculation of minibands is based on the evaluation of sub-band energies through the finite difference method. Finally, in order to show the trend of changing the minibands and minigaps more clearly, when the number of wells, inner or outer QD (or QR) radius changes, we add two moving pictures (.gif files), too.

In the present work, we have studied the effect of a hydrogenic donor impurity and the number of wells on the miniband formation process in GaN/AlN CTER-MSQDs and CTER-MSQRs. Our calculation of minibands is based on the evaluation of sub-band energies through a finite difference method. Finally, to show the trend of changing the minibands and minigaps more clearly, when the number of wells, inner or outer QD (or QR) radius changes, we have also provided two moving pictures, see supplementary files.

2 Formalism

Behavior of electrons in quantum dots can be described by means of radial part of the spherical Schrödinger equation within the effective mass approximation by

$$\left[-\frac{\hbar^2}{2m^*}\left(\frac{\partial^2}{\partial r^2}+\frac{2}{r}\frac{\partial}{\partial r}-\frac{L(L+1)}{r^2}\right)-\frac{e^2}{4\pi\varepsilon r}+V(r)\right]\times\psi(r)=E. \quad (1)$$

For quantum rings in cylindrical coordinates we have

$$\left[-\frac{\hbar^2}{2m^*}\left(\frac{\partial^2}{\partial \rho^2}+\frac{1}{\rho}\frac{\partial}{\partial \rho}-\frac{M_z^2}{\rho^2}\right)-\frac{e^2}{4\pi\varepsilon\rho}+V(\rho)\right]\times\psi(\rho)=E\psi, \quad (2)$$

where m^* is the effective mass and $V(r)$ is the geometrical confining potential which defined by

$$V(r)=\begin{cases}V_{conf} & i=1,3,\ldots \\ 0 & i=2,4,\ldots\end{cases};\ \frac{i-1}{2N+1}R_1<r<\frac{i}{2N+1}R_2, \quad (3)$$

Equation (3) illustrates the shape of the quantum well that confines the free carriers such as electrons. For electrons, it is equal to the conduction band discontinuity at an interface in a quantum hetero-structure. For illustration purposes we have presented a schematic representation of a typical single-well quantum ring system in Figure 1 and depict the potential profile versus radius r.

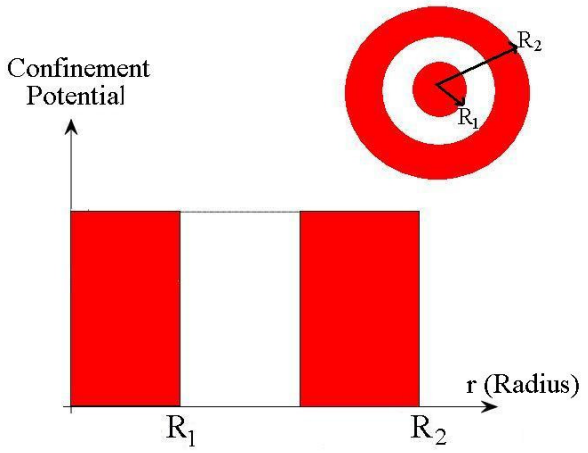

Figure 1: Schematic representation of a typical single-well quantum ring system. Here we have depicted the potential profile versus radius.

We can also define the potential in the same manner. Here, N is the number of wells, V_{conf} is the constant relative conduction band offset and i shows the i^{th} well or barrier. M_z =0, ±1, ±2…, is the magnetic quantum numberwhile L is the orbital quantum number. We have used a finite difference method [27] to solve Eqs. (1) and (2). We have previously checked the accuracy of the used method [29].

3 Results and discussion

We have used GaN/AlN CTELSs because of their lattice-match with crystal structures. We assume the effective mass values as $m^* = 0.12m_e$ and $0.48m_e$ for GaN and AlN semiconducting systems, respectively [28]. The confinement potential is taken equal to 1.28eV [28]. The given values for the outer radii are considered equal to 400, 600, and 1000 Å while for the inner radii are considered equal to 0, 350, 500, and 750 Å. Note that in the system the inner radius equal to 750 Å corresponds to the outer radius equal to 1000 Å. We have also supposed that all wells and barriers in a system have the same thickness, e.g. in three-well CTER-MSQDs we have three wells and four barriers which have the same thickness.

We have solved the Schrödinger equations (1) and (2) using the finite difference method to obtain the energy eigenvalues (sub-band energies) and the corresponding eigenvectors. In Figure 2, we have plotted the variation of the sub-band energies as a function of the quantum dot radius for a spherical CTER-MSQD. The outer QD radius has been taken as R_2=1000 Å while the inner QD radius has been take as R_1=0 Å. The three panels of Figure 2 respectively correspond to three different orbital quantum numbers (L) equal to 0, 1, and 2, where the minibands and minigaps are clearly shown. Figures 2a and 2b which correspond to L=0 and L=1 show four minibands and three minigaps while in Figure 2c which corresponds to L=3 shows five minibands and four minigaps. Variation of the minibands and minigaps is not monotonic when the number of wells increases. There is a unique trend in all three panels of Figure 2. When the number of wells increases, minigaps appear where by further increasing the number of wells they disappear.

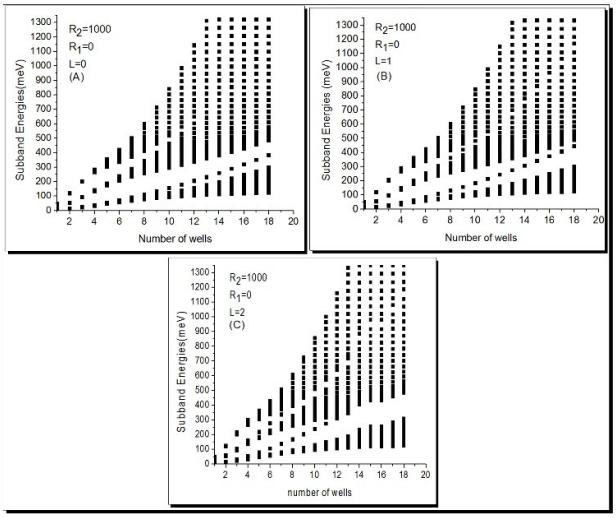

Figure 2. Minibands and minigaps of a spherical CTER-MSQD with outer QD radius R_2=1000 Å, inner QD radius R_1=0 Å, and with orbital quantum numbers L=0, 1, and 2 respectively corresponding to panels a, b, and c.

This is true for all magnetic quantum number M_z and L. However, since we have only increased the number of wells up to 20, some minigaps, the second and third, in Figure 2A have not disappeared. We did not increase the number of wells more, because fabricating the very thin quantum wells and barriers is not possible experimentally. Note that, since we have kept the outer quantum dot radius (R_2) constant while at the same time have increased the number of wells, thus by increasing the number of wells, the wells and barriers thicknesses decrease. In the meantime, there is not a general statement about the maximum width of the minigaps and minibands; as it seems their behavior has not a concrete rule. For example, the widest minigaps in Figures 2a and 2b are the second ones while in Figure 2c the first minigap is the widest one.

This is not the behavior we usually see in usual superlattices. In usual superlattices, when the number of wells increases, the width of each miniband and minigap increases where after reaching a maximum value remain constant. In the three panels of Figure 2, we have chosen the maximum value of the vertical axis to be equal to 1300meV because the confinement potential for the GaN/AlN heterostructures is equal to 1.28eV as mentioned earlier. Thus, we can choose a special spherical CTER-MSQD with special number of wells to have a system with a special number of miniband and miniband widths. Now, each number of minibands and miniband widths can be achieved for a

special heterostructure like GaN/AlN just by varying the number of wells. However, to enable more choices when we need a system with a special number of minibands and miniband widths, we have changed the QD and QR radii. One might as well remove the impurity. Recently [26], we have done this by studying the procedure of miniband formation in CTER-MSQDs. Roughly speaking, in the presence of the hydrogenic donor impurity, we can have systems with bigger minigapgs.

Now, if we choose the outer QD radius (R_2) equal to 1000 Å and inner QD radius (R_1) equal to 0 A° we will have a cylindrical QD. We have shown the minibands and minigaps of a cylindrical CTER-MSQD with magnetic quantum numbers M_z=0, 1, and 2 in panels a, b, and c of Figure 3. If we compare Figure 2a with Figure 3a we see that the spherical CTER-MSQDs have one miniband more than the cylindrical CTER-MSQD. But, the minibands of the cylindrical CTER-MSQD are wider. Generally speaking, variation of the minibands and minigaps is not monotonic when the number of wells increases. However, in panels a and b of Figure 3, we see that for systems with number of wells greater than eight, the first minigap width is approximately fixed but its position is blue shifted, this is also true for cylindrical systems, see e.g. Figures 5 and 7),

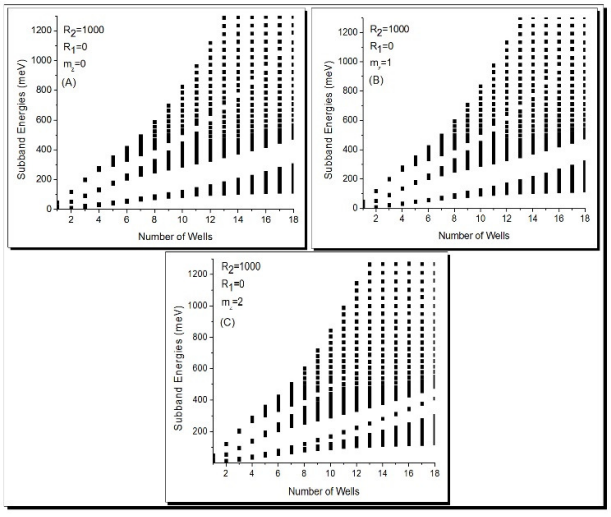

Figure 3. Minibands and minigaps of a cylindrical CTER-MSQD with outer QD radius R_2=1000 Å, inner QD radius R_1=0 Å, and with magnetic quantum numbers M_z=0, 1 and 2 respectively corresponding to panels a, b, and c.

In the following we shall see that this fact is true for cylindrical systems while for spherical systems there is not a general statement. In panels a and b of Fgure 3, for M_z =0 and M_z =1, there are three minibands and two minigaps but for Mz =3 it could be seen in panel c of Figure 3 that there are four minibands and three minigaps.

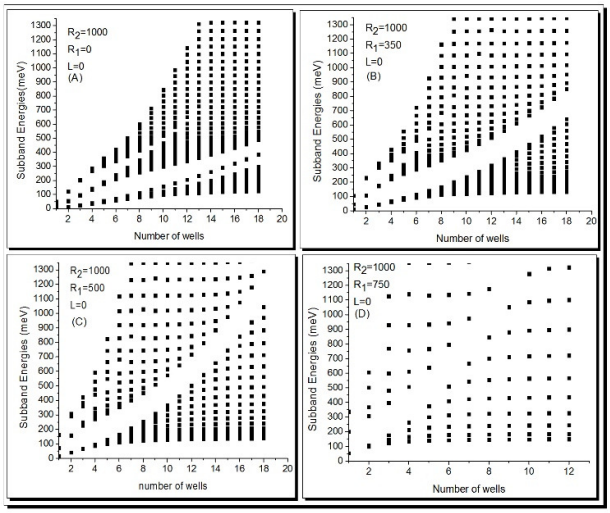

Figure 4. Minibands and minigaps of a spherical CTER-MSQD with QD outer radius R_2=1000 , orbital quantum number L=0 and inner QD radius R_1=0 Å, 350 Å, 500 Å, and 750 Å respectively presented in a, b, c, and d.

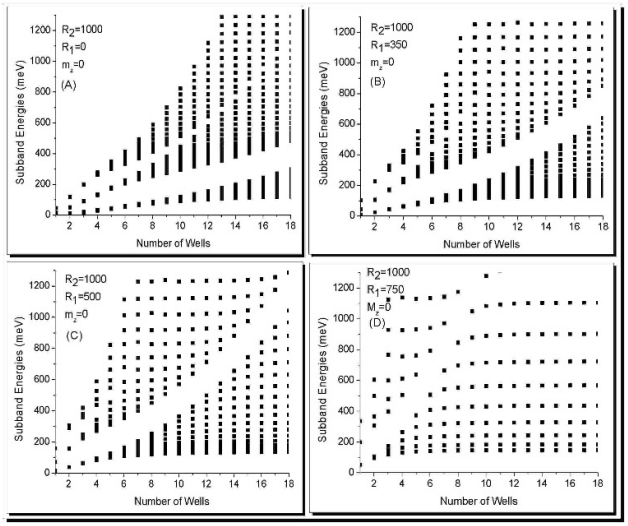

Figure 5. Minibands and minigaps of a CTER-MSQR with outer QR radius R_2=1000 Å, magnetic quantum numbers M_z=0, and inner QR radius R_1=0 Å, 350 Å, 500 Å, and 750 respectively presented in panels a, b, c, and d.

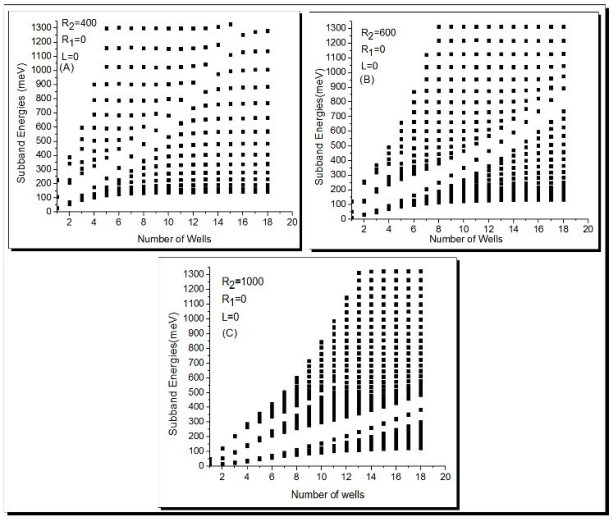

Figure 6. Minibands and minigaps of a spherical CTER-MSQD with QD inner radius R_1=0 Å, orbital quantum numbers L=0, and outer QD radius R_2=400 Å, 600 Å, and 1000 Å ° respectively presented in panels a, b, and c.

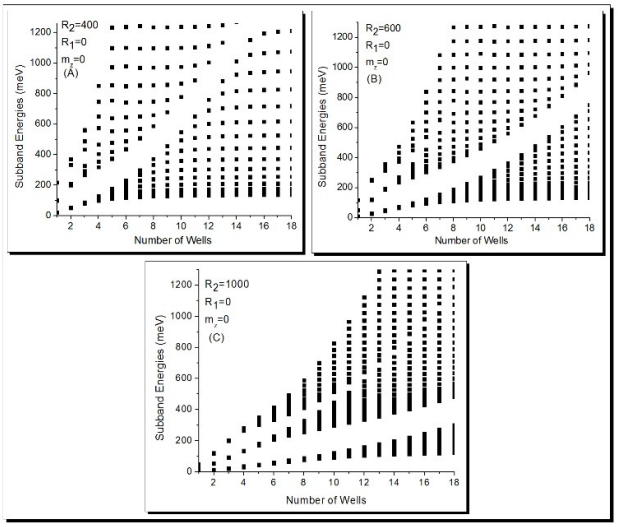

Figure 7. Minibands and minigaps of a cylindrical CTER-MSQD with inner QD radius R_1=0 Å, magnetic quantum numbers M_z=0, and outer QD radius R_2=400 Å, 600 Å, and 1000 Å respectively presented in panels a, b, and c.

At this time, for the spherical CTER-MSQD, we choose the outer QD radius (R_2) equal to 1000 Å and orbital quantum numbers (L) equal to 0. Then, we show the minibands and minigaps of the systems with different inner QD radius, R_1=0 Å, 350 Å, 500 Å, and 750 Å in panels a, b, c, and d of Figure 4, respectively. As we can see, by increasing the inner quantum dot radius R_1, the minibands turn into some discrete sub-band energy levels (compare different panels of Figure 4). Another fact is that by increasing the inner quantum dot radius R_1, the number of minibands gradually decreases. The number of minigaps in Figures 4a-4d is equal to 3, 2, 1, and 0, respectively. Here, we have calculated the minibands and minigaps of a CTER-MSQR with outer QR radius (R_2)=1000 Å, magnetic quantum numbers M_z=0, and inner QR radius R_1=0 Å, 350 Aº, 500 Å, and 750 Å. The results are shown in panels a, b, c, and d of the Figure 5, respectively. Now, the number of minigaps in Figures 5a-5d is equal to 2, 2, 1, and 1, respectively. As we can see in these panels, the width of the first minigap in CTER-MSQRs is independent of the inner quantum dot reduces. This means that the behavior of the minibands is somewhat dependent on the shape of the quantum dot. Just as in Figure 3 (but here for systems with number of wells greater than six), the first minigap width is approximately fixed but its position has is shifted. Here, there is a difference.

In Figure 3, the amount of blue shift in the position of the minigap is the same for panels a and b. This means that magnetic quantum numbers M_z do not change the amount of blue shift too much. However, in Figure 5, we see that the first minigap position undertakes much blue shift when the inner QD radius R_1 increases. This is consistent with the elementary quantum mechanical intuition which says that energy levels of a quantum well increases by decreasing the well width. e.g. for an infinite quantum well: energy levels are: $E_n = n^2 p^2 \mathrm{h}^2 / 2mL^2$, where L is the well width.

Now, we study the effect of the outer QD radius R_2 on the miniband formation scenario. Figure 6 shows the minibands and minigaps of a spherical CTER-MSQD with QD inner radius (R_1) equal to 0 Å, orbital quantum numbers L=0, and outer QD radius R_2=400 Å, 600 Å, and 1000 Å presented in panels a, b, and c, respectively. In contrast to Figure 4, by decreasing the outer quantum dot radius R_2, the minibands turn into some discrete sub-band energy levels (compare different panels of Figure 6). This is because, both when we increase the inner QD radius (R_1) at fixed outer QD radius R_2, or when we decrease the outer QD radius (R_2), at fixed inner QD radius R_1, we will have narrower quantum wells in the studied system. At this time we study the cylindrical QDs. Figure 7 shows the minibands and minigaps of a cylindrical CTER-MSQD with inner QD radius (R_1) equal to 0 Å, magnetic

quantum numbers M_z=0, and outer QD radius R_2=400 Å, 600 Å and 1000 Å in panels a, b and c, respectively. Just like Figure 6, by decreasing the outer quantum dot radius (R_2), the minibands turn into some discrete sub-band energy levels (compare different panels of Figure 7). Just as before, if we compare Figures 6 and 7, we see that the spherical CTER-MSQDs have one miniband more than cylindrical CTER-MSQDs. For more illustration purposes about the scenario of the miniband formation and the effects of different parameters on this phenomenon, we have also included two moving picture files, see supplementary file.

4 Conclusions

In the current work, the miniband formation procedure in GaN/AlN CTER-MSQDs and CTER-MSQRs under the influence of the hydrogenic donor impurity and the number of wells was investigated by sub-band energy calculations. We showed that when the number of wells increases, minigaps create where by further increasing the number of wells they annihilate. This was true for all magnetic quantum number M_z and L. There was not a general statement about the maximum width of the minigaps and minibands as it seems their behavior have not a concrete rule. In the presence of the hydrogenic donor impurity, we could have systems with bigger minigapgs. Cylindrical CTER-MSQDs have one miniband more than spherical CTER-MSQD. But, the minibands of the cylindrical CTER-MSQD are wider. For cylindrical systems with the number of wells greater than a critical value, the first minigap width is approximately fixed when the number of wells increases as its position experiences a blue-shift. But for spherical systems, there is not a general statement. By increasing the inner quantum dot radius (R_1), the minibands turn into some discrete sub-band energy levels while at the same time, the number of minibands gradually decrease. The first minigap position undertakes a large blue shift when the inner QD radius R_1 increases. Thus, the number of wells, hydrogenic donor impurity, and quantum dot & ring radii could be used as a tuning tools to have a system with the special number of miniband and miniband widths.

Acknowledgments

We are grateful for the supports of the Qom University of Technology.

References

[1] L. Esaki, "A bird's-eye view on the evolution of semiconductor superlattices and quantum wells" IEEE Journal of Quantum Electronics, **QE-22** (1986) 1611.

[2] L. Esaki, R. Tesu, "Superlattice and Negative Differential Conductivity in Semiconductors." IBM Journal of Research and Development, **14** (1970) 61.

[3] L. Esaki, L. L. Chang, "Quantum States of Confined Carriers in Very Thin $Al_xGa_{1-x}As$-GaAs-$Al_xGa_{1-x}As$ Heterostructures." Physical Review Letters, **33** (1974) 495.

[4] L. Esaki, "Long journey into tunneling." Science, **183** (1974) 1149.

[5] J. W. Klos, M. Krawczyk, "Electronic miniband formation in a two-dimensional semiconductor superlattice." Materials Science-Poland, **26** (2008) 965.

[6] U. Behn, N. Linder, H. T. Grahn and K. Ploog, " Investigation of miniband formation in a graded-gap superlattice by electroreflectance spectroscopy." Physical Review B, **51** (1995) 17271.

[7] M. Holthaus, "Collapse of minibands in far-infrared irradiated superlattices." Physical Review Letters, **69** (1992) 351.

[8] X.-G. Zhao, "Phonon-induced collapse of minibands in superlattices." Physics Letters A, **230** (1997) 229.

[9] Yu. A. Pusep, A. J. Chiquito, S. Mergulhao, and J. C. Galzerani , "One-dimensional character of miniband transport in doped GaAs/AlAs superlattices." Physical Review B, **56** (1997) 3892.

[10] P. Hyldgaard and A. P. Jauho, " Elastic and inelastic resonant tunnelling in narrow-band systems: application to transport in minibands of semiconductor superlattices." Journal of Physics: Condensed Matter, **2** (1990) 8725.

[11] Y. Shimada, K. Hirakawa, and S-W Lee, "Time-resolved terahertz emission spectroscopy of wide miniband GaAs/AlGaAs superlattices." Applied. Physics Letters, **81** (2002) 1642.

[12] H. T. Grahn, K. von Klitzing, and K. Ploog, G. H. Dohler, "Electrical transport in narrow-miniband semiconductor superlattices." Physical Review B, **43** (1991) 12094.

[13] S-Y Cheng, W-C Liu, W-L Chang, H-J Pan, W-C Wang, J-Y Chen, S-C Feng, and K-H Yu, " Observation of the impulse-like negative-differential resistance of superlatticed resonant-tunneling transistor." Applied. Physics Letters, **75** (1999) 133.

[14] M. A. Green, "Third generation photovoltaics: solar cells for 2020 and beyond." Physica E, **14** (2002) 65.

[15] F. Fuchs, E. Ahlswede, U. Weimar, W. Pletschen, and J. Schmitz, M. Hartung and B. Jager, F. Szmulowicz, "Magneto-optics of InAs/$Ga_{1-x}In_xSb$ infrared superlattice diodes." Applied. Physics Letters, **73** (1998) 3760.

[16] S. Tortora , F. Compagnone , A. Di Carlo, P. Lugli, "Theoretical study, modeling and simulation of SL quantum cascade lasers." Physica E **7** (2000) 20.

[17] E. Plis, S. J. Lee, Z. Zhu, A. Amtout, and S. Krishna, "InAs/GaSb superlattice detectors operating at room temperature." IEEE Journal of Selected Topics in Quantum Electronics, **12** (2006) 1269.

[18] X-B Cai, X-F Xuan, "Optical harmonic generation in a Fibonacci dielectric superlattice of $LiNbO_3$." Optics Communications, **240** (2004) 227.

[19] X. I. Saldana, D. A. Contreras-Solorio, E. Lopez-Cruz, "Self-similar optical properties in Pascal-Type quasiperiodic dielectric multilayer." Revista Mexicana de Fisica S, **53** (2007) 310.

[20] D. K. Ferry, S. M. Goodnick, J. Bird, "Transport in Nanostructures, Second Edition, Cambridge University Press", New York, 2009.

[21] P. Harrison, Quantum Wells, Wires and Dots, "Theoretical and Computational Physics of Semiconductor Nanostructures, Second Edition, John Wiley & Sons, LTD", San Francisco, 2005.

[22] M. Solaimani, M. Izadifard, H. Arabshahi, and M. R. Sarkardei, "Study of optical non-linear properties of a constant total effective length multiple quantum wells system." Journal of Luminescence **134** (2013) 699.

[23] M. Solaimani, "GaN/AlN constant total effective radius multi-wells quantum rings: physical properties under well number variation effects" Solid State Communications, **200** (2014) 66.

[24] M. Solaimani, "Nonlinear optical absorption of a two electron GaN/AlN constant total effective radius multi-shells quantum rings" Journal of Nonlinear Optical Physics and Materials, **23** (2014) 1450050.

[25] M. Solaimani, M. Ghalandari, L. Lavaie, "Donor impurity effects on optical properties of GaN/AlN constant total effective radius multishell quantum dots" Journal of the Optical Society of America B, **33** (2016) 420.

[26] M. Solaimani, "Miniband formation in GaN/AlN constant-total-effective-radius multi-shell quantum dots" Chinese Physics Letters, **32** (2015) 117304.

[27] M. V. K. Chari, S. J. Salon, "Numerical Methods in Electromagnetism, Academic Press", Maryland, 2000.

[28] I. Vurgaftman, J. R. Meyer and L. R. Ram-Mohan, " Band parameters for III–V compound semiconductors and their alloys" Journal of Applied Physics, **89** (2001) 5815.

[29] M. Solaimani, "Osscillating Binding Energy of a Donor Impurity Confined Within CdS-SiO2 Constant Total Effective Radius Multi-Shells Quantum Dots." International Journal of Nanoscience, **15** (2016) 1650003.